HHS Public Access

Author manuscript

NMR Biomed. Author manuscript; available in PMC 2017 July 01.

Published in final edited form as:

NMR Biomed. 2016 July ; 29(7): 896–903. doi:10.1002/nbm.3536.

Spatiotemporal changes in diffusion, T2 and susceptibility of white matter following mild traumatic brain injury

Wei Li[1,2,+], **Justin Alexander Long**[1,+], **Lora Watts**[+], **Qiang Shen**, **Yichu Liu**, **Zhao Jiang**[1], and **Timothy Q. Duong**[1,2,*]

[1]Research Imaging Institute, University of Texas Health Science Center at San Antonio, TX 78229, USA

[2]Department of Ophthalmology, University of Texas Health Science Center at San Antonio, TX 78229, USA

Abstract

Impaired white matter integrity in traumatic brain injury (TBI) can lead to deficits in various neurological functions. Differentiation of the underlying pathological processes, e.g. edema, demyelination, axonal damage to name a few, is of key clinical interest for assessing white matter injury. In this study, a combination of T_2, diffusion and susceptibility MRI were used to study the spatiotemporal changes in white matter at 1 hour, 3 hours, 1, 2, 7, and 14 days following TBI, using a rat controlled cortical impact (CCI) model. Based on radial diffusivity (RD), the rats were divided into two groups: group 1 showed widespread increases of RD along the corpus callosum of the ipsilesional hemisphere at day 2, and group 2 showed normal RD. Based on this group separation, group 1 also showed similar widespread changes of fractional anisotropy (FA) and T_2 at day 2, and group 2 showed normal FA and T_2. The widespread changes in RD and T_2 in group 1 on day 2 were apparently dominated by edema, which obscured possible myelin and axonal damage. In contrast, the susceptibility of group 1 showed more localized increases near the impact site on day 2, and otherwise similar contrast to the contralesional hemisphere. The localized susceptibility increase is likely due to demyelination and axonal injury. The extent of brain damage between the two groups revealed by MRI was consistent with behavioral results where the first group showed significantly increased forelimb asymmetry and increased forelimb foot fault deficits. Our results suggest that the combination of T_2, diffusion and susceptibility MRI may provide an opportunity for differential assessment of edema and axonal damage in TBI.

Graphical Abstract

[*]**Correspondence address:** Timothy Duong, PhD, duongt@uthscsa.edu, Research Imaging Institute, Department of Ophthalmology, University of Texas Health Science Center at San Antonio, TX 78229, USA.

[+]Wei Li, Justin Long and Lora Watts made equal contributions to this study.

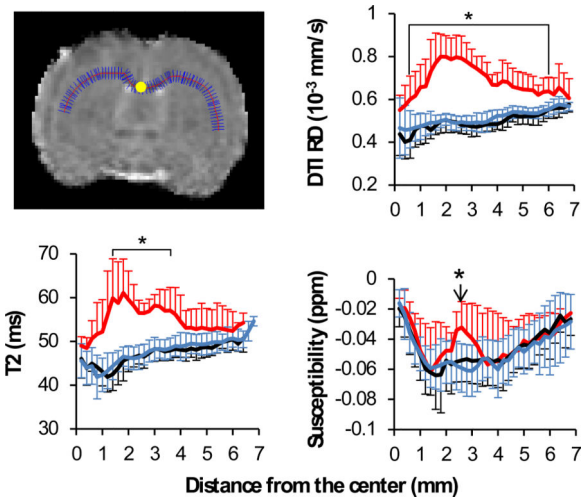

T_2, diffusion and susceptibility MRI were used to study the spatiotemporal changes in white matter following traumatic brain injury, using a rat controlled cortical impact model. Two groups of animals were differentiated: group 1 showed widespread changes in T_2 and diffusion in the ipsilesional hemisphere at day 2, and group 2 showed no changes. The widespread changes in T_2 and diffusion in group 1 were dominated by edema. The localized susceptibility increase was likely due to myelin and axonal damages.

Keywords

Traumatic brain injury; white matter; quantitative susceptibility mapping; diffusion tensor imaging; T_2 mapping

Introduction

Traumatic brain injury (TBI) is one of the most common causes of death and disability in young people (1). An estimated 1.7 million people suffer from TBI annually in the United States (2). TBI is a complex injury with a broad spectrum of symptoms and cognitive impairments, e.g. headache, dizziness, fatigue, depression, etc. (3). A TBI patient's cognitive impairment is often inadequately explained by the location and extent of the injury (4). One of the reasons may be due to diffuse white matter damage that disrupts neuronal communication along important cortical-subcortical pathways and leads to widespread cognitive dysfunction (5,6). The extent of white matter damage has been suggested as an important predictor of brain injury severity and long-term clinical outcome (7,8). White matter damage can be caused by the primary insult or by the cascade of secondary injuries due to electrolyte imbalances, energy failure, and inflammation, among others (9,10). Various methods have been proposed to attenuate white matter injury as a treatment for TBI (11,12). The knowledge of the spatiotemporal changes in white matter following TBI is crucial for improving diagnosis of TBI, and for evaluating treatment effects.

Neuroimaging methods, e.g. T_2-weighted MRI and diffusion tensor imaging (Strother, #2927) (6), have provided powerful tools for the study of white matter in TBI (6,13). T_2-

weighted signal changes are sensitive to edema formation. DTI parameters, e.g. fractional anisotropy (FA), mean diffusivity (MD) and radial diffusivity (RD), are sensitive to demyelination, axonal damage and edema. The impact of demyelination and further axonal damage can cause permanent and severe neurological deficits. However, the assessment of myelination and axonal integrity by DTI FA and mean diffusivity can be significantly confounded by cerebral edema. Over the past few years, a novel MRI method, quantitative susceptibility mapping (QSM) (14–22), has shown a unique sensitivity to white matter damage (23–26), in addition to deoxygenated and degraded blood (27,28). A previous study reported that white matter dysmyelination led to an almost complete absence of phase and susceptibility contrast between gray and white matter in a transgenic Shiverer mouse model, which was compared to only moderately altered DTI contrasts (23). Subsequent studies showed that the susceptibility contrast between gray and white matter was directly related to myelin lipid content, along with orientation factors (29). These studies suggest that magnetic susceptibility could provide a potentially useful marker to study myelin or axonal damage in TBI.

In this study, we evaluated the spatiotemporal changes in diffusion, T_2 and magnetic susceptibility of the corpus callosum, one of the major white matter fiber tracks, at 1 hour, 3 hours, 1, 2, 7, and 14 days following TBI, using an established rat controlled cortical impact (CCI) model. The diffusion, T_2 and susceptibility changes of the corpus callosum at different time points were evaluated by projecting the maximum or minimum values of RD, FA, T_2 and magnetic susceptibility along the corpus callosum. Based on RD images, the animals were easily divided into two groups. These two groups showed dramatically different diffusion, T_2 and susceptibility changes, which, taken together, provide novel insights into the evolution of edema, myelin or axonal damage in white matter during the acute and sub-acute phases of TBI.

Materials and Methods

Controlled cortical impact (CCI) model of mild TBI

All animal procedures were approved by the Institutional Animal Care and Use Committee of the University of Texas Health Science Center at San Antonio. Experimental TBI was done as previously described (30,31). Briefly, male Sprague Dawley rats (250–350g, n=18) were anesthetized initially with 5% isoflurane mixed with room air and maintained at 1.2% isoflurane throughout all surgical and imaging procedures. The animal was secured in a stereotaxic frame and a surgical incision was made posterior to the impact site (at the level of the cerebellum) and the periosteum was removed over the impact site. A ∅5mm craniotomy was created over the left forelimb primary somatosensory cortex (S1FL: +0.25mm anterior and 3.5mm lateral to bregma), exposing the dura matter. The intact dura matter was impacted using a pneumatic controlled cortical impactor (Precision Systems and Instrumentation, LLC, Fairfax Station, Virginia) fitted with a ∅3mm tip (5.0m/s, 250μs dwell time, 1mm depth) to mimic a mild focal TBI. Following the impact the cranial opening was sealed with bone wax, the scalp sutured closed and antibiotic ointment applied. Saline was injected between the scalp and the skull to minimize artifacts during MRI acquisition.

MRI

The rats were scanned using a Bruker 7T scanner 1hr, 3hrs, 2, 7 and 14 days after TBI. The heart rate and blood-oxygen saturation level were also monitored using a MouseOx system (STARR Life Science, Oakmont, PA, USA).

Diffusion Tensor imaging (3.5 min): DTI images were acquired using a single-shot spin-echo echo-planar imaging sequence with partial Fourier (5/8). A single low b-value image of 10 s/mm^2 and 30 gradient directions with a b-value of 1200 s/mm^2 were acquired using the following parameters: seven 1.0-mm coronal images, Field of view (FOV) = 2.56 × 2.56 cm, matrix 96 × 96 and reconstructed to 128 × 128, TR = 3 s, TE = 32 ms, and 2 averages.

T_2 mapping (9.5 min): T_2-weighted images were acquired using a fast spin-echo sequence with TR = 3 s (90° flip angle), effective TE = 18, 54, 90 and 126 ms, 4 echo train length. Other parameters were: seven 1.0-mm coronal images, FOV = 2.56 × 2.56 cm, matrix 96 × 96 and reconstructed to 128 × 128 and 8 averages. T_2 map was obtained by linear fitting of the natural logarithm of the signal intensity versus TE.

Quantitative susceptibility mapping (11.5 min): QSM data were acquired using a 3D multi-gradient echo sequence with the following parameters: FOV=2.56×2.56×2.56cm^3, data matrix=256×192×128, TE1=4.4ms, Echo spacing=6.1ms, 4 echoes, and TR=28ms. The raw data was saved and exported for further offline analysis.

Data Analysis

DTI data was analyzed as previously described (32). The RD was calculated as the mean radial diffusivity. QSM was performed using a software package for QSM and susceptibility tensor imaging (STI), which is called “STI Suite” (33). Briefly, the brain image was reconstructed with 3D Fast Fourier transform. The complex data was separated into magnitude and phase. The magnitude image from the third echo was used for the extraction of the brain tissue. The phase images from the four different echoes were unwrapped using Laplacian-based unwrapping (16) and summed. The background phase was removed as described in reference (21). The tissue susceptibility was determined as described in reference (16). The resulting magnetic susceptibility values were directly used for comparison (34).

To evaluate MRI contrast along the white matter tracts and to eliminate the subjectivity of manual region of interest selection, we projected the maximum values of RD, T_2 and magnetic susceptibility, and the minimum values of FA along the corpus callosum. The choice of the minimum values for FA was because of the hypointensity of FA associated with the white matter damage. The choice of RD over MD was due to its better differentiation between white matter water and cerebrospinal fluid (CSF). RD is calculated as the mean of two radial diffusivities, both of which are much smaller than the diffusivity of CSF. As such, RD provides excellent differentiation between white matter and CSF, which is a prerequisite for the projection analysis approach used in this study. In contrast, the axial diffusivity (AD) in white matter is not much different from that of the CSF, therefore is incompatible with this type of analysis. Since MD also contains contributions of AD (MD = 2/3 RD +1/3 AD), it was also not selected for analysis. Figure 1A shows an example of the

analysis of RD, in which the maximum values of RD along the short blue lines were projected along the center of the corpus callosum (the red line). The resulting profile of RD along the corpus callosum is shown in Figure 1B. Such an approach was used to minimize the potential partial volume effect due to the small fraction of white matter in the rodent brain. The projected values were compared across different time points. All the programs for data analysis were written using Matlab R2011b (Mathworks, Natick, MA), using a desktop computer with an Intel Core i7-4700 ™ CPU and 32GB RAM.

The objective of this study was to differentiate white matter edema and axonal injury in TBI using MRI. From Figure 1B, RD showed either widespread increases along the corpus callosum or no change at all. While the normal RD indicates intact white matter, the widespread RD increases can reflect a combination of edema and axonal injury. We hypothesized that susceptibility MRI may provide useful information to separate axonal injury from widespread edema. To evaluate this hypothesis, the animals were separated into two groups based on RD profiles shown in Figure 1B: group 1 showed widespread increases in RD along the corpus callosum (red solid lines, n=6), and group 2 showed normal RD (gray solid lines, n=12). The RD profiles of the two groups were so different that there was no ambiguity in the separation of the groups. Since RD was used as the sole criteria, the group separation did not impact with the analysis of T_2 and susceptibility.

Behavioral assessment

Sensorimotor function was assessed using the asymmetry forelimb placement (cylinder) test and foot-fault test, which have been shown to have appropriate sensitivity for this injury model (30). Testing was conducted 1–3 days prior to TBI and again 1, 2, 7, and 14 days post TBI. The forelimb asymmetry placement test was performed to assess the use of the forelimbs during exploration of the cylinder. The rat was placed in a transparent cylinder (20cm diameter, 30cm height) and videotaped for five minutes or until 30 placements were made. The behavior was scored by counting the number of left right individual forelimb placements and the number of simultaneous left and right forelimb placements onto the wall of the cylinder during rearing. The forelimb asymmetry index was calculated as (the number of forelimb placements for each individual limb) + 0.5 × (number of both placements) divided by the total number of placements. The forelimb foot fault test was performed to assess forelimb misplacement during locomotion. The rat was placed on an elevated grid floor (size 18×11 inches with grid openings of 1.56 × 1.00 inches) and videotaped for five minutes or until 50 steps were taken with one (non-affected) forelimb. The rat was allowed to move freely on the grid and the total number of steps and the number of times each limb fell below the grid opening were counted. The percentage of foot faults for each limb were calculated as the number of right or left forelimb foot faults divided by the total number of steps taken.

Black Gold II histology

Black Gold II (Histo-Chem Inc. Jefferson, Arkansas, USA) was utilized to assess damage to myelin in the central nervous system in an additional 4 animals. Black Gold II stain is a gold-based salt that has been shown to specifically stain myelin. This dye was chosen based on its ease of use and higher contrast and resolution of staining compared to lipid soluble

dyes and antibodies directed towards myelin (35). Anesthetized rats were perfused with ice-cold heparinized phosphate buffered saline, followed by ice-cold 4% buffered paraformaldehyde on day 14 post-TBI. Brains were removed and fixed for 2–5hrs at 4°C and subsequently cryopreserved in 30% sucrose for 48 hours. Coronal sections 25-μm thick) were cut on a cryostat and affixed to gelatin coated slides and dried overnight at 37°C. Sections were selected based on susceptibility maps. The selected sections were rehydrated in distilled water and then transferred to a heated 0.3% Black Gold II (Milipore) solution prepared in 0.9% NaCl. The sections were placed in an oven at 65 °C for 12 minutes (or until sufficient staining was achieved). The slides were then washed with distilled Milli-Q water and then transferred to 1% sodium thiosulfate for three minutes. The slides were then rinsed for 15 minutes in running tap water. The slides were then dehydrated using graduated alcoholic solutions and finally immersed in histoclear for 2 minutes a cover slipped with DPX mounting media. Images were acquired on an Olympus BX60F microscope equipped with an Olympus DP70 camera. A 10× objective was utilized to acquire images for mosaic full brain images assimilated using Microsoft ICE software.

Statistical analysis

Values are presented as mean ± standard derivation. Standard unpaired t-tests were used to compare T_2, radial diffusivity, and FA between the two groups and between the ipsi- and contra-lesional sides. Bonferroni correction was used to correct for the effect of multiple comparisons. $p<0.05$ between group 1 and group 2, and between group 1 ipsilesional and contralateral were highlighted as statistically significant changes.

Results

Widespread diffusion/T_2 alterations vs localized magnetic susceptibility increases

Figure 2 shows the representative RD, FA, T_2 and susceptibility maps of white matter 2 days after TBI. Consistent with increased RD, group 1 also showed increased T_2, increased susceptibility and decreased FA in the corpus callosum. In contrast, group 2 showed normal T_2, susceptibility and FA throughout the corpus callosum. The observed different patterns of T_2, FA and susceptibility between the two groups further confirmed the validity of group separation.

Figure 3 showed the spatiotemporal profiles of RD, FA, T_2, and susceptibility along the corpus callosum. For this TBI model, the RD, FA and T_2 were normal at 1 hour, 3 hour, day 7 and day 14, except that the corpus callosum of group 1 showed a local T_2 increase in a very small region on day 7. On day 2, the corpus callosum of group 1 showed widespread increases in RD and T_2, and widespread decreases in FA. In particular, the RD increase was almost across the entire ipsilesional side of the corpus callosum. For group 1, the magnetic susceptibility of the ipsilesional side of the corpus callosum showed a localized increase at 2.6 mm from the center of corpus callosum (bottom row of Figure 3). The magnetic susceptibility at other locations along the corpus callosum was similar to the contralesional side. For group 2, the RD, FA, T_2 and magnetic susceptibility of the corpus callosum all remained the same when compared to that of the contralesional side.

Behavioral studies of the two groups

As shown in Figure 4, overall, TBI led to increased front limb asymmetry and an increase in the number of forelimb foot faults that recovered to nearly normal on day 14 for both groups. Between the groups, group 1 showed significantly increased front limb asymmetry at day 2 and day 7, and significantly more forelimb foot faults at day 2, day 7 and day 14 compared to group 2.

Comparison between QSM and histology

Figure 5 shows the comparison between susceptibility maps and white matter staining using Black Gold II in two TBI rats on day 2 post-injury. There was a decrease in the magnetic susceptibility contrast in the impacted hemisphere most notably in the corpus callosum directly below the impact site as shown in Figure 5A and B and noted by yellow arrows as a loss of intensity. Corresponding sections stained with Black Gold II are illustrated in Figure 5C and D. In these images it is clear that the impacted corpus callosum had a loss of staining and suggested a loss of myelin associated with white matter damage. Magnified images also demonstrated the loss of staining particularly within the corpus callosum (shown by the yellow arrows) when compared to the contralesional corpus callosum (shown by the green arrows) (Figure 5 E and F). The data illustrates that QSM can detect loss of white matter staining and corresponds to the same regions where myelin loss was evident in Black Gold II stained tissue.

Discussion

In this study, we separated the mild TBI rats into two groups based on the profiles of RD along the corpus callosum, and compared the spatiotemporal changes in diffusion, T_2 and magnetic susceptibility between the two groups. Group 1 showed widespread changes in RD, FA and T_2 on day 2, and localized increases in magnetic susceptibility on the ipsilesional side of the corpus callosum; group 2 showed normal contrasts throughout all time points. These MRI data suggested that the group 1 has more damage to the brain white matter than group 2, which agrees with increased forelimb asymmetry and increased forelimb faults of group 1 animals than group 2.

Diffusion and T_2 changes in corpus callosum

From RD and the T_2 images, it was apparent that the widespread changes in RD, FA, and T_2 in group 1 were dominated by cerebral edema. It can be also seen that white matter edema can propagate much easier into the gray matter. This can be explained by structural differences between the gray and white matter. The white matter axonal fibers are much more loosely packed than the neuronal bodies and dendrites in the gray matter. If the injury is limited to the gray matter, edema will be restricted to a smaller region. If the injury penetrates the gray matter and reaches the white matter, the edema will be spread through a much larger region. Similar to the gray matter edema, the white matter edema also peaked at day 2, and was gradually absorbed (30). Knowledge of edema formation is useful for predicting the increase of intracranial pressure. However, it will also obscure the detection of myelin and axonal damage. To obtain the myelin and axon information in the presence of widespread edema, advanced diffusion methods, such as higher order diffusion tensors (36)

and diffusion basis spectrum imaging (37), will be required. However, such methods will take significantly longer scan times, and sophisticated post-processing methods.

Susceptibility changes in white matter

The aforementioned shiverer mice study suggested that susceptibility MRI may provide higher sensitivity and specificity to changes in myelin compared to DTI (23). These could be attributed to the fact that diffusion and susceptibility contrasts are related to different aspects of white matter structures. DTI FA and ADC are related to the hindered diffusion of water molecules due to the cellular barriers (38). The relationship between FA/ADC and myelin content can be highly nonlinear, so that a very low myelin content in shiverer mice only lead to moderate changes in FA and ADC (23). In contrast, the susceptibility of white matter is linearly related to the myelin lipid fraction, along with orientation factors (29,39,40). Due to this linear relationship, much more dramatic reduction of phase and susceptibility contrast between gray and white matter were observed in shiverer mice (23). Different sensitivities of susceptibility, FA and ADC to myelin has also been reported in a study of the developing mouse brain (26). Based on these previous studies, the local increase in susceptibility observed in this study is likely attributable to a corresponding reduction in myelin, which was further supported by myelin staining using Black Gold II. Since the white matter damage in this model was caused by mechanical impact, it is unlikely that only myelin was affected and axonal structure was intact, and it is more likely that the observed susceptibility increases could reflect damage to both myelin and axons.

In addition to myelin, edema is also expected to alter the susceptibility of white matter, since it reduces the fraction of the diamagnetic myelin. Previously, it has been reported that water content increases by 12% and 42% in vasogenic and osmotic edema of the white matter due to cold induced injury (41). This can lead to increased magnetic susceptibility of white matter, since myelin is more diamagnetic relative to water. However, in most of the white matter regions with increased RD and T_2, no such increases were observed. It is possible that edema-related susceptibility changes are smaller compared to physiological variations. This also suggested that the localized susceptibility increase at day 2 corresponds to significant myelin and axonal damage. Previous studies of mouse models of multiple sclerosis suggested that demyelination and remyelination are slower processes compared to edema formation and absorption, and can take a few days to even weeks to complete (42). While susceptibility and diffusion changes are only observed on day 2 in our model, some degree of myelin and axonal damage could also exist at other time points. Further histological studies at other time points will be needed to establish the degree of white matter damage detectable by MRI.

Although the current results suggest that the combination of T_2, diffusion and susceptibility MRI may have the potential to disentangle the effects of edema and myelin damage, a few limitations of QSM processing should be noted. Firstly, QSM required removal of background phase, which eliminates the reference for calculating the absolute tissue frequency shift and magnetic susceptibility. Currently, there is still no gold standard to select the susceptibility reference, therefore, the susceptibility values after QSM are directly used for comparisons. This method essentially sets the susceptibility reference to the mean

susceptibility value of the whole brain tissue (34). Secondly, the magnetic susceptibility of white matter is also dependent on the sine square of the fiber angle with respect to the main magnetic field (29,40,43). However, measurement of the full susceptibility tensor requires the rotation of the brain inside the scanner (40,43,44), which is difficult to perform. In the current experimental setup, the selected corpus callosum regions were nearly perpendicular to the main magnetic field with the maximum contrast between gray and white matter. Third, phase and susceptibility are also dependent on all image acquisition parameters (45), due to the differential frequency and T_1 and T_2 relaxations between different water compartments of the white matter (46,47). This multi-compartment can also introduce orientation dependent effects on top of susceptibility anisotropy (48). Another limitation is that histology was performed in a small subgroup of only 4 animals.

Correlation with behavioral analyses

Forelimb asymmetry and forelimb foot fault behavioral tests were used as a means of detecting functional outcomes of this TBI model. The T_2, diffusion, and magnetic susceptibility changes in group 1 were in agreement with the significantly increased forelimb asymmetry and increased number of forelimb foot faults when compared to group 2. These results could suggest a link between white matter damage and functional outcomes. However, this finding should be considered in light of other confounding factors. Particularly, this study focused on the white matter, while the degree of gray matter damage was not examined. It is also possible that group 1 has more severe gray matter damage as well. Finally, the sensitivity of these behavioral tests may not be high enough to detect more subtle fine motor function deficits. Further assessment of the impact of white matter injury on functional outcome would require the inclusion of a significantly larger number of animals, increased sensitivity of behavioral outcome measures, and robust statistical analysis to control for the degree of gray matter damage.

Conclusions

Based on RD, two groups of animals could be separated: group 1 that showed widespread changes in RD at day 2, and group 2 showed normal RD at all the time points. FA and T_2 showed similar widespread (group 1) or no (group 2) changes similar to RD. These widespread changes were attributable to the dominance of white matter edema, which obscured the contrast of other pathological processes. In contrast, susceptibility of group 1 showed localized increases at day 2, which is likely due to the myelin and axonal injury. Behaviorally, the white matter damage in group 1 agreed with the increased deficits seen with forelimb asymmetry and forelimb fault functional outcome measures. Collectively, our results suggest that T_2, diffusion and susceptibility provide a combination to differentiate edema and myelin or axonal damage in TBI.

Acknowledgments

This work was supported in part by NIH/NINDS R01 NS45879 (TQD). The project described was also supported by the National Center for Advancing Translational Sciences, National Institutes of Health, through Grant KL2 TR001118 (LTW). W.L. was also supported in part by UL1 TR001119 via the Clinical Translational Science Awards (CTSA), and a research grant from William & Ella Owens Medical Research Foundation.

List of abbreviations

CCI	controlled cortical impact
DTI	diffusion tensor imaging
FA	fractional anisotropy
FOV	field of view
MD	mean diffusivity
QSM	quantitative susceptibility mapping
RD	radial diffusivity
TBI	traumatic brain injury

References

1. Coronado VG, McGuire LC, Sarmiento K, Bell J, Lionbarger MR, Jones CD, Geller AI, Khoury N, Xu L. Trends in Traumatic Brain Injury in the U.S. and the public health response: 1995–2009. J Safety Res. 2012; 43(4):299–307. [PubMed: 23127680]
2. Faul, M.; Xu, L.; Wald, M.; Coronado, VG. Traumatic brain injury in the United States: emergency department visits, hospitalizations and deaths 2002–2006. Atlanta, GA: Centers for Disease Control and Prevention, National Center for Injury Prevention and Control; 2010. p. 2-70.
3. Stålnacke, B-m; Björnstig, U.; Karlsson, K.; Sojka, P. One-year follow-up of patients with mild traumatic brain injury: post-concussion symptoms, disabilities and life satisfaction at follow-up in relation to serum levels of S-100B and neuron-specific enolase in acute phase. Journal of Rehabilitation Medicine. 2005; 37(5):300–305. [PubMed: 16208863]
4. Bigler ED. The lesion (s) in traumatic brain injury: Implications for clinical neuropsychology. Archives of Clinical Neuropsychology. 2001; 16(2):95–131. [PubMed: 14590180]
5. Kinnunen KM, Greenwood R, Powell JH, Leech R, Hawkins PC, Bonnelle V, Patel MC, Counsell SJ, Sharp DJ. White matter damage and cognitive impairment after traumatic brain injury. Brain. 2010:awq347.
6. Kraus MF, Susmaras T, Caughlin BP, Walker CJ, Sweeney JA, Little DM. White matter integrity and cognition in chronic traumatic brain injury: a diffusion tensor imaging study. Brain. 2007; 130(10): 2508–2519. [PubMed: 17872928]
7. Benson RR, Meda SA, Vasudevan S, Kou Z, Govindarajan KA, Hanks RA, Millis SR, Makki M, Latif Z, Coplin W. Global white matter analysis of diffusion tensor images is predictive of injury severity in traumatic brain injury. Journal of neurotrauma. 2007; 24(3):446–459. [PubMed: 17402851]
8. Sidaros A, Engberg AW, Sidaros K, Liptrot MG, Herning M, Petersen P, Paulson OB, Jernigan TL, Rostrup E. Diffusion tensor imaging during recovery from severe traumatic brain injury and relation to clinical outcome: a longitudinal study. Brain. 2008; 131(2):559–572. [PubMed: 18083753]
9. Meythaler JM, Peduzzi JD, Eleftheriou E, Novack TA. Current concepts: diffuse axonal injury–associated traumatic brain injury. Archives of physical medicine and rehabilitation. 2001; 82(10): 1461–1471. [PubMed: 11588754]
10. Morganti-Kossmann MC, Rancan M, Otto VI, Stahel PF, Kossmann T. Role of cerebral inflammation after traumatic brain injury: a revisited concept. Shock. 2001; 16(3):165–177. [PubMed: 11531017]
11. Pu H, Guo Y, Zhang W, Huang L, Wang G, Liou AK, Zhang J, Zhang P, Leak RK, Wang Y, Chen J, Gao Y. Omega-3 polyunsaturated fatty acid supplementation improves neurologic recovery and attenuates white matter injury after experimental traumatic brain injury. J Cereb Blood Flow Metab. 2013; 33(9):1474–1484. [PubMed: 23801244]

12. Park KJ, Park E, Liu E, Baker AJ. Bone marrow-derived endothelial progenitor cells protect postischemic axons after traumatic brain injury. J Cereb Blood Flow Metab. 2014; 34(2):357–366. [PubMed: 24301295]
13. Ashikaga R, Araki Y, Ishida O. MRI of head injury using FLAIR. Neuroradiology. 1997; 39(4): 239–242. [PubMed: 9144669]
14. de Rochefort L, Liu T, Kressler B, Liu J, Spincemaille P, Lebon V, Wu JL, Wang Y. Quantitative susceptibility map reconstruction from MR phase data using Bayesian regularization: validation and application to brain imaging. Magn Reson Med. 2010; 63(1):194–206. [PubMed: 19953507]
15. Kressler B, de Rochefort L, Liu T, Spincemaille P, Jiang Q, Wang Y. Nonlinear regularization for per voxel estimation of magnetic susceptibility distributions from MRI field maps. Medical Imaging, IEEE Transactions on. 2010; 29(2):273–281.
16. Li W, Wu B, Liu C. Quantitative susceptibility mapping of human brain reflects spatial variation in tissue composition. Neuroimage. 2011; 55:1645–1656. [PubMed: 21224002]
17. Shmueli K, de Zwart JA, van Gelderen P, Li TQ, Dodd SJ, Duyn JH. Magnetic susceptibility mapping of brain tissue in vivo using MRI phase data. Magn Reson Med. 2009; 62(6):1510–1522. [PubMed: 19859937]
18. Liu T, Spincemaille P, de Rochefort L, Kressler B, Wang Y. Calculation of susceptibility through multiple orientation sampling (COSMOS): a method for conditioning the inverse problem from measured magnetic field map to susceptibility source image in MRI. Magnetic Resonance in Medicine. 2009; 61(1):196–204. [PubMed: 19097205]
19. Wharton S, Schafer A, Bowtell R. Susceptibility mapping in the human brain using threshold-based k-space division. Magn Reson Med. 2010; 63(5):1292–1304. [PubMed: 20432300]
20. Liu T, Liu J, de Rochefort L, Spincemaille P, Khalidov I, Ledoux JR, Wang Y. Morphology enabled dipole inversion (MEDI) from a single-angle acquisition: Comparison with COSMOS in human brain imaging. Magnetic Resonance in Medicine. 2011; 66(3):777–783. [PubMed: 21465541]
21. Wu B, Li W, Guidon A, Liu C. Whole brain susceptibility mapping using compressed sensing. Magn Reson Med. 2012; 67(1):137–147. [PubMed: 21671269]
22. Schweser F, Deistung A, Lehr BW, Reichenbach JR. Quantitative imaging of intrinsic magnetic tissue properties using MRI signal phase: an approach to in vivo brain iron metabolism? Neuroimage. 2011; 54(4):2789–2807. [PubMed: 21040794]
23. Liu C, Li W, Johnson GA, Wu B. High-field (9.4 T) MRI of brain dysmyelination by quantitative mapping of magnetic susceptibility. Neuroimage. 2011; 56(3):930–938. [PubMed: 21320606]
24. Lee J, Shmueli K, Kang B-T, Yao B, Fukunaga M, van Gelderen P, Palumbo S, Bosetti F, Silva AC, Duyn JH. The contribution of myelin to magnetic susceptibility-weighted contrasts in high-field MRI of the brain. NeuroImage. 2012; 59(4):3967–3975. [PubMed: 22056461]
25. Lodygensky GA, Marques JP, Maddage R, Perroud E, Sizonenko SV, Hüppi PS, Gruetter R. In vivo assessment of myelination by phase imaging at high magnetic field. NeuroImage. 2012; 59(3):1979–1987. [PubMed: 21985911]
26. Argyridis I, Li W, Johnson GA, Liu C. Quantitative magnetic susceptibility of the developing mouse brain reveals microstructural changes in the white matter. NeuroImage. 2014; 88(0):134–142.
27. Wang Y, Liu T. Quantitative susceptibility mapping (QSM): Decoding MRI data for a tissue magnetic biomarker. Magnetic Resonance in Medicine. 2015; 73(1):82–101. [PubMed: 25044035]
28. Liu C, Li W, Tong KA, Yeom KW, Kuzminski S. Susceptibility-weighted imaging and quantitative susceptibility mapping in the brain. Journal of Magnetic Resonance Imaging. 2015; 42(1):23–41. [PubMed: 25270052]
29. Li W, Wu B, Avram AV, Liu C. Magnetic susceptibility anisotropy of human brain in vivo and its molecular underpinnings. Neuroimage. 2012; 59(3):2088–2097. [PubMed: 22036681]
30. Long JA, Watts LT, Chemello J, Huang S, Shen Q, Duong TQ. Multiparametric and longitudinal MRI characterization of mild Traumatic Brain Injury in rats. Journal of neurotrauma. 2014; 32(8): 598–607. [PubMed: 25203249]

31. Watts LT, Long JA, Chemello J, Van Koughnet S, Fernandez A, Huang S, Shen Q, Duong TQ. Methylene Blue Is Neuroprotective against Mild Traumatic Brain Injury. Journal of neurotrauma. 2014; 31(11):1063–1071. [PubMed: 24479842]
32. Shen Q, Ren H, Fisher M, Bouley J, Duong TQ. Dynamic Tracking of Acute Ischemic Tissue Fates Using Improved Unsupervised ISODATA Analysis of High-Resolution Quantitative Perfusion and Diffusion Data. Journal of Cerebral Blood Flow & Metabolism. 2004; 24(8):887–897. [PubMed: 15362719]
33. Li W, Avram AV, Wu B, Xiao X, Liu C. Integrated Laplacian-based phase unwrapping and background phase removal for quantitative susceptibility mapping. NMR in Biomedicine. 2014; 27(2):219–227. [PubMed: 24357120]
34. Li W, Wu B, Batrachenko A, Bancroft-Wu V, Morey RA, Shashi V, Langkammer C, Bellis MDD, Ropele S, Song AW, Liu C. Differential developmental trajectories of magnetic susceptibility in human brain gray and white matter over the lifespan. Human Brain Mapping. 2014; 35(6):2698–2713. [PubMed: 24038837]
35. Schmued L, Bowyer J, Cozart M, Heard D, Binienda Z, Paule M. Introducing Black-Gold II, a highly soluble gold phosphate complex with several unique advantages for the histochemical localization of myelin. Brain Research. 2008; 1229:210–217. [PubMed: 18657520]
36. Liu C, Mang SC, Moseley ME. In vivo generalized diffusion tensor imaging (GDTI) using higher-order tensors (HOT). Magnetic Resonance in Medicine. 2010; 63(1):243–252. [PubMed: 19953513]
37. Wang Y, Wang Q, Haldar JP, Yeh F-C, Xie M, Sun P, Tu T-W, Trinkaus K, Klein RS, Cross AH. Quantification of increased cellularity during inflammatory demyelination. Brain. 2011; 134(12): 3590–3601. [PubMed: 22171354]
38. Basser PJ, Mattiello J, Lebihan D. MR diffusion tensor spectroscopy and imaging. Biophysical Journal. 1994; 66(1):259–267. [PubMed: 8130344]
39. Lounila J, Alakorpela M, Jokisaari J, Savolainen MJ, Kesaniemi YA. Effects of orientational order and particle-size on the NMR line positions of lipoproteins. Physical Review Letters. 1994; 72(25):4049–4052. [PubMed: 10056366]
40. Li W, Liu C. Comparison of Magnetic Susceptibility Tensor and Diffusion Tensor of the Brain. Journal of Neuroscience and Neuroengineering. 2013; 2(5):431–440. [PubMed: 25401058]
41. Go KG, Edzes HT. Water in brain edema: observations by the pulsed nuclear magnetic resonance technique. Archives of neurology. 1975; 32(7):462–465. [PubMed: 1137512]
42. Matsushima GK, Morell P. The Neurotoxicant, Cuprizone, as a Model to Study Demyelination and Remyelination in the Central Nervous System. Brain Pathology. 2001; 11(1):107–116. [PubMed: 11145196]
43. Liu C, Li W, Wu B, Jiang Y, Johnson GA. 3D Fiber tractography with susceptibility tensor imaging. Neuroimage. 2012; 59(2):1290–1298. [PubMed: 21867759]
44. Liu C. Susceptibility tensor imaging. Magn Reson Med. 2010; 63(6):1471–1477. [PubMed: 20512849]
45. Li W, Han H, Guidon A, Liu C. Dependence of gradient echo phase contrast on the differential signal decay in subcellular compartments. Proc Int Soc Magn Reson Med. 2013; 21
46. Wharton S, Bowtell R. Fiber orientation-dependent white matter contrast in gradient echo MRI. Proceedings of the National Academy of Sciences. 2012; 109(45):18559–18564.
47. Sati P, van Gelderen P, Silva AC, Reich DS, Merkle H, de Zwart JA, Duyn JH. Micro-compartment specific T2* relaxation in the brain. NeuroImage. 2013; 77(0):268–278. [PubMed: 23528924]
48. Wharton S, Bowtell R. Effects of white matter microstructure on phase and susceptibility maps. Magnetic Resonance in Medicine. 2013; 73(3):1258–1269. [PubMed: 24619643]

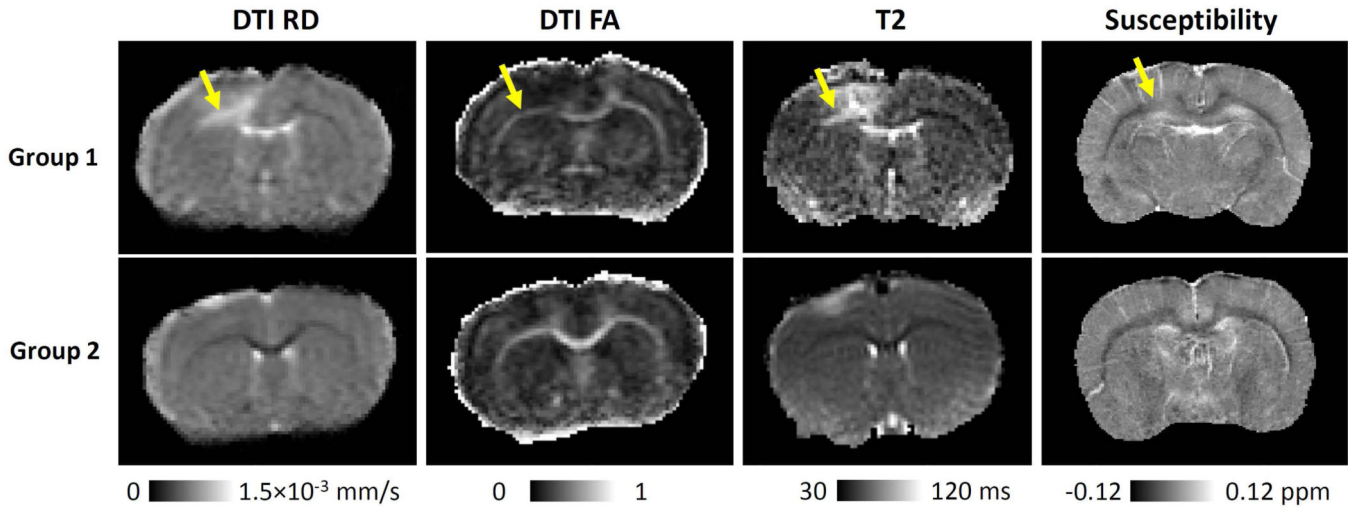

Figure 1.

The projection of white matter contrast along the corpus callosum. A: a representative projection for diffusion RD. The maximum RD value along the short blue lines was used as the RD value along the center of corpus callosum as outlined by the red line. The center of corpus callosum is labeled as the yellow dot. B: the profile of RD along corpus callosum based on the distance from the center of the corpus callosum in mm. Red solid lines: group 1 (n=6). Gray solid lines: Group 2 (n=12).

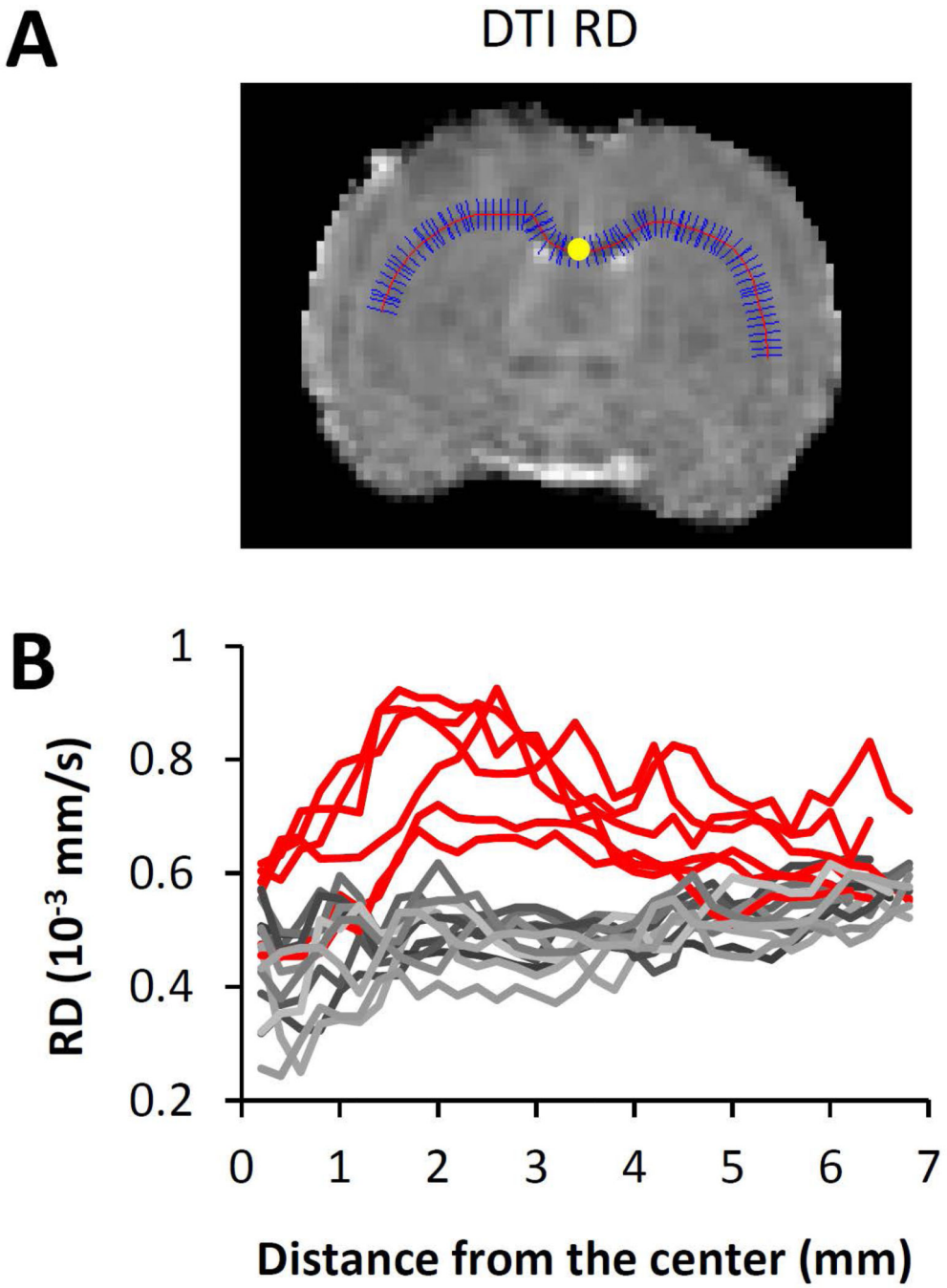

Figure 2.

Representative diffusion, T_2 and susceptibility images of the TBI rats for group 1 (n=6, upper row) and group 2 (n=12, lower row). The white arrow pointed to the increased RD, T_2, decreased FA and increased magnetic susceptibility. The yellow arrow pointed out the white matter abnormalities in group 1.

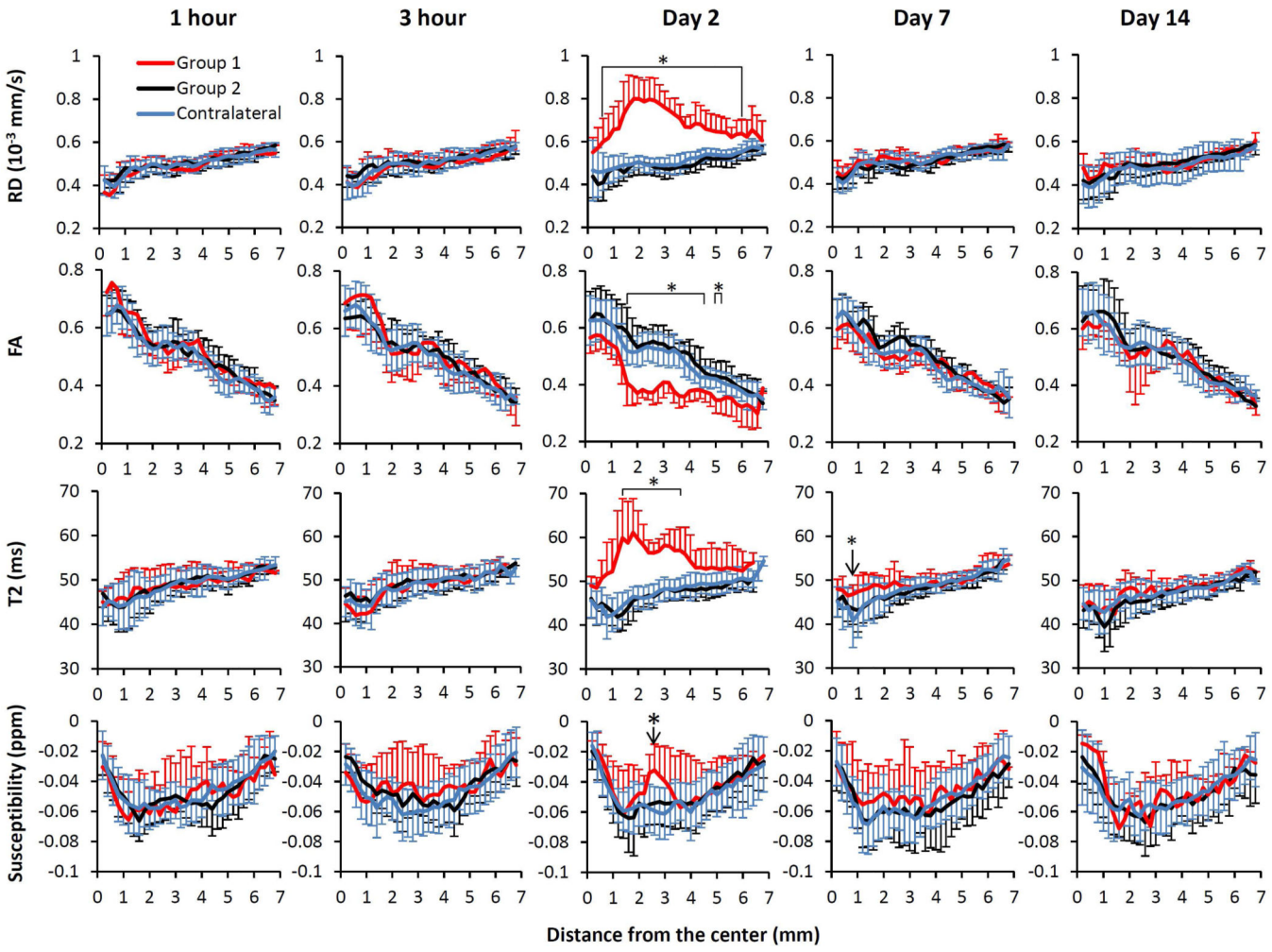

Figure 3.

Spatiotemporal changes in RD, FA, T_2 and susceptibility values at 1 hour, 3 hours, 2 days, 7 days and 14 days based on the distance from the center of the corpus callosum in mm.. *p<0.05 between group 1 (n=6) and group 2 (n=12) ipsilesional values, and between group 1 ipsilesional and contralateral hemispheres.

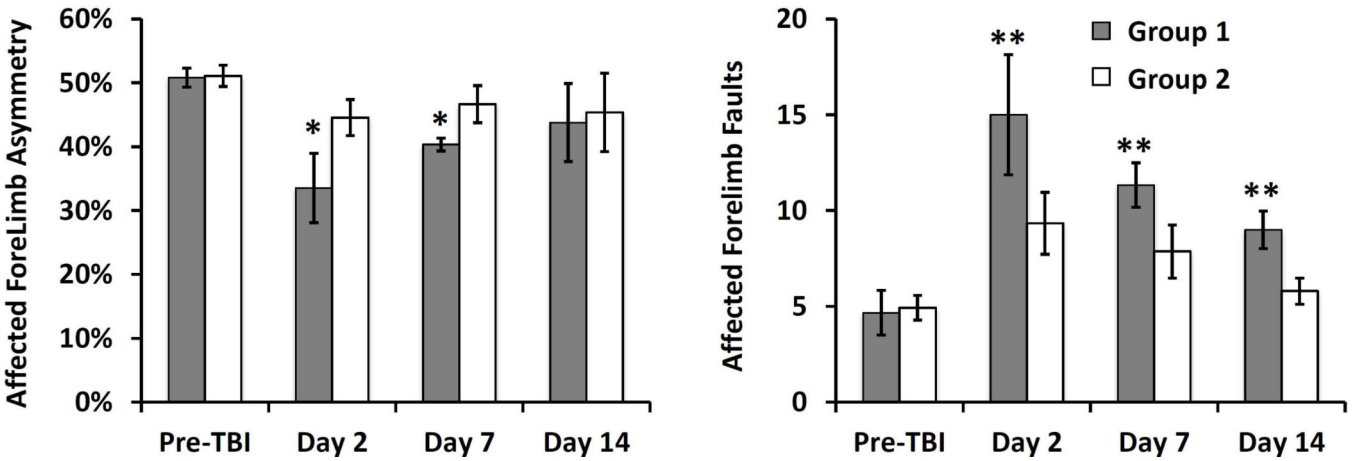

Figure 4.

Comparison of behavior performance between the two groups prior to the induction of TBI and at 2 days, 7 days and 14 days post-TBI. *p<0.05 and **P<0.01 between groups 1 (n=6) and group 2 (n=12). Data are represented as mean ± standard deviation. All behavioral scores after TBI were significantly different from those of pre-TBI in both groups except the asymmetry at day 14 for both groups and day 7 in group 2, and foot fault on day 14 of group 2.

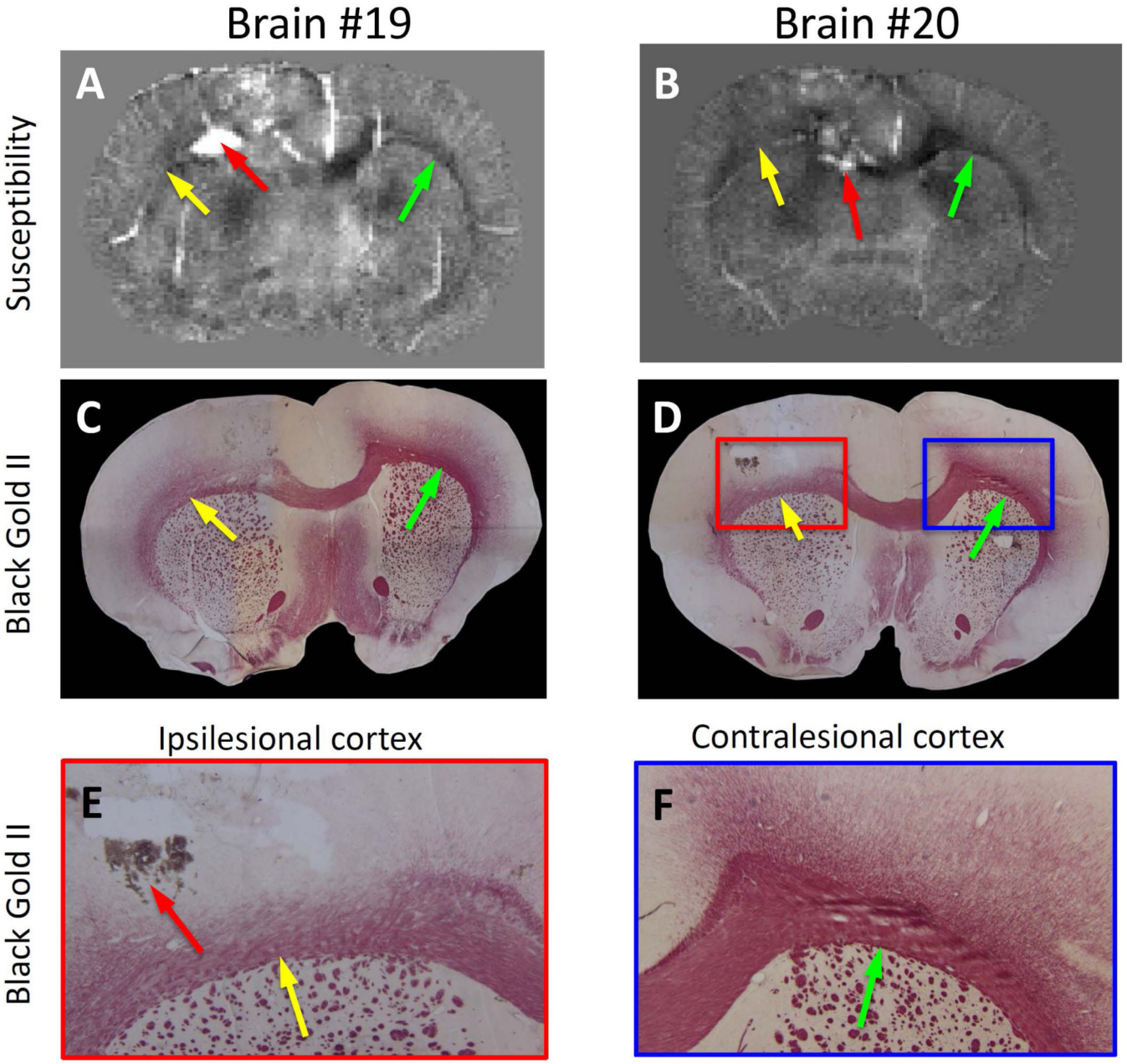

Figure 5.

Comparison of magnetic susceptibility with white matter histology. A and B: magnetic susceptibility for two different rat brains. C and D: myelin staining using Black Gold II of the same rat brains as A and B. E and F: Zoom in images of the ipsilesional and contralesional images of the histology shown in D. Yellow arrow: ipsilesional. Green arrow: contralesional. The red arrow pointed to hemorrhages resulted from the controlled cortical impact.